Intrinsic second-order topological insulators produced by triangular Kekulé distortion in honeycomb lattices

Yixuan Gao,[1] Lizhi Zhang,[2,*] Yu-Yang Zhang,[3] and Shixuan Du[3,4,†]

[1]*State Key Laboratory for Advanced Metals and Materials, University of Science and Technology Beijing, Beijing 100083, China*
[2]*National Center for Nanoscience and Technology, Chinese Academy of Sciences, Beijing 100190, China*
[3]*Institute of Physics & University of Chinese Academy of Sciences, Chinese Academy of Sciences, Beijing 100190, China*
[4]*Songshan Lake Materials Laboratory, Dongguan 523808, China*

(Received 15 November 2023; revised 24 June 2024; accepted 7 August 2024; published 3 September 2024)

Chiral symmetry breaking (CSB) is promising to realize a series of exotic topological phenomena due to the coupling of Dirac fermions at inequivalent valleys. We propose a strategy to introduce CSB by applying a Kekulé distortion in a spinless honeycomb lattice, resulting in the emergence of a second-order topological phase as the period of the superlattice is $3m \times 3m$ ($m = 1, 2, \ldots$). Following the strategy, Si_xC_y and circumcoronene-based two-dimensional (2D) honeycomb lattices are predicted to be second-order topological insulators (SOTIs) that are identified via the topological invariants and the presence of in-gap topological corner modes. In this paper, we provide an effective approach to realize CSB in a honeycomb lattice and greatly enrich 2D SOTIs families.

DOI: 10.1103/PhysRevB.110.125103

I. INTRODUCTION

High-order topological insulators (TIs) have special bulk-boundary correspondence [1–6], where, the nth ($n = 2, 3, \ldots$)-order TI in d dimensions has protected gapless states on its $(d - n)$-dimensional boundaries. For example, a second-order TI (SOTI) in two dimensions (2D) [three dimensions (3D)] hosts topological states at its zero-dimensional (0D) corners [one-dimensional (1D) hinges] within their gapped edge (surface) states. SOTIs have stimulated great interest due to hosting symmetry-protected gapless states, which are promising for spintronic devices [7,8]. Up to now, 2D SOTIs can be produced by four different theoretical models. (I) The time-reversal-symmetry-breaking model destroys the first-order topological phase while protecting the second-order topological phase by introducing magnetism [9,10]. (II) The band-inversion model inverts bands with opposite parities twice [11]. (III) The breathing lattice model results in the mismatch between the atom sites and the Wannier centers in square and kagome lattices [3,12]. (IV) The Kekulé distorted model breaks chiral symmetry in honeycomb lattices [13,14].

Kekulé-distortion-induced chiral symmetry breaking (CSB) is the result of coupling of Dirac fermions with opposite chiralities at valleys K and K' and the corresponding gap opening [15–22]. Though two Kekulé distortions (Kekulé-Y or Kekulé-O) with a superlattice period of $(\sqrt{3} \times \sqrt{3})$R30° in a honeycomb lattice have been reported [19,22–24], only Kekulé-O distortion can induce gap opening, thus realizing CSB and showing high-order topological states [13,14,25–32]. We notice that the coupling of Dirac fermions with opposite chiralities can also be realized in distorted $(3m \times 3m)$ ($m = 1, 2, \ldots$) superlattices due to the two valleys being folded into Γ [21]. Thus, it opens opportunities for investigating CSB-induced 2D SOTIs based on distorted $3m \times 3m$ superlattices.

In this paper, we introduce a triangular Kekulé distortion (namely, Kekulé-T) in honeycomb lattices with superlattice period of $(3m \times 3m)$, where $m = 1, 2, \ldots$. Based on the tight-binding (TB) models, we predict the existence of second-order topological phases in $(3m \times 3m)$ superlattices by applying Kekulé-T distortion. We find that the two valleys K and K' are folded into Γ, lead to gap opening and resulting in SOTIs. By using first-principles calculations, we predict two categories of group-IV materials to be SOTIs, i.e., 2D Si_xC_y and the circumcoronene-based covalent organic framework (COF). The SOTI characteristics of these materials are identified via their topological invariants and the presence of in-gap topological corner modes. We also predict that a first-order topological phase exists in 2D Si_xC_y with superlattice periods of $[(3m + l) \times (3m + l)]$, when $l = 1$ or 2. In this paper, we provide a systematic strategy to design 2D SOTIs and first-order TIs (FOTIs) in honeycomb lattices.

II. RESULTS

Previous reported Kekulé-O and Kekulé-Y distortions are both based on a $(\sqrt{3} \times \sqrt{3})$R30° superlattice [22,24], where Kekulé-O distortion could introduce a band gap, while Kekulé-Y distortion has been revealed to keep gapless band structure [33]. The Kekulé distortion originated from a distinct bond order within hexagonal rings. Thus, the TB model of Kekulé distortion is reflected by the different nearest-neighbor (NN) hopping parameters. Here, we introduce a typical Kekulé-T distortion in honeycomb lattices and construct NN TB models on three honeycomb lattices with periods of $(N \times N)$ ($N = 3$, 4, and 5), as shown in Figs. 1(a)–1(c). There are three types of hopping in each unit cell, i.e., t_1, t_2, and t_3, marked by gray, red, and dashed red lines, respectively.

*Contact author: zhanglz@nanoctr.cn
†Contact author: sxdu@iphy.ac.cn

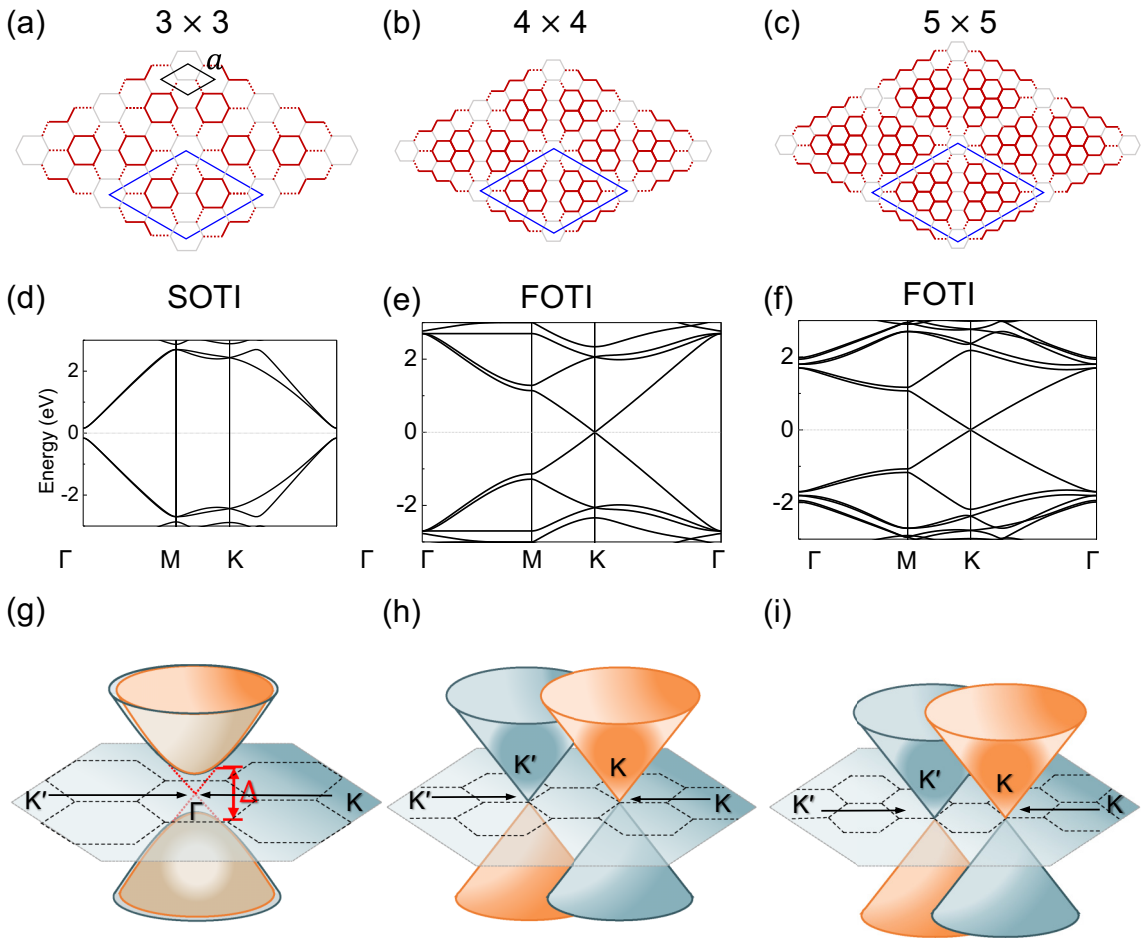

FIG. 1. Classification of two-dimensional (2D) Kekulé-T lattice with D_{6h} symmetry. (a)–(c) Sketch of the 2D Kekulé-T lattice with different bond strengths (represented by gray, red, and red dashed lines) in different sizes (unit cell periods equal to 3, 4, and 5). The unit cells are marked by blue rhombus. The a is the lattice constant of a honeycomb lattice in the absence of distortion, as shown in black rhombus in (a). (d)–(f) Band structures by using tight-binding models with $N = 3$, 4, and 5, respectively. The parameters are set as $t_1 = -2.70\,\text{eV}$, $t_2 = -3.00\,\text{eV}$, and $t_3 = -3.25\,\text{eV}$. (g)–(i) Schematic of band folding.

The lattice constants are $3a$, $4a$, and $5a$ in three honeycomb lattices, respectively, where a is the lattice constant of a honeycomb lattice in the absence of distortion.

The TB model is built based on a single orbital as follows:

$$\hat{H} = t_1 \sum_{ij} (\hat{c}_i^\dagger \hat{c}_j + \text{H.c.}) + t_2 \sum_{i'j'} (\hat{c}_{i'}^\dagger \hat{c}_{j'} + \text{H.c.}) + t_3 \sum_{i''j''} (\hat{c}_{i''}^\dagger \hat{c}_{j''} + \text{H.c.}).$$

In the model, only NN hopping between the orbitals is considered. The TB parameters are set to be $t_1 = -2.70\,\text{eV}$, $t_2 = -3.00\,\text{eV}$, and $t_3 = -3.25\,\text{eV}$.

The energy dispersions of three Kekulé-T distorted honeycomb lattices are shown in Figs. 1(d)–1(f). The system with a period of (3×3) opens a gap at the Γ point, while the systems with periods of (4×4) and (5×5) remain gapless. The energy dispersion of systems with periods of (6×6), (7×7), and (8×8) shows the same characteristics as shown in Fig. S2 in the Supplemental Material (SM) [34]. According to the energy band folding, these superlattices can be categorized into two groups on the basis of the Dirac cone position, as schematically illustrated in Figs. 1(g)–1(i). In the cases of the superlattice with a period of (3×3), the intervalley coupling of a Dirac fermion with opposite chiralities at K and K' leads to CSB, which replicate Dirac cones at the Brillouin zone center (Γ point) and gap opening. In the cases of superlattices with periods of (4×4) and (5×5), the K and K' points in primitive cells correspond to that in the superlattices. Therefore, K and K' remain twofold degenerate Dirac points. These two systems belong to FOTIs due to an odd total parity of all time-reversal invariant momenta (TRIM), leading the calculated $\mathbb{Z}_2$ invariants to both equal 1.

The CSB in the system is promising to realize high-order topological states [14,28]. Since Kekulé-T distorted honeycomb lattices have both P and T symmetries, the higher-order band topology of the system with a period of (3×3) can be characterized by second Stiefel-Whitney number ω_2. The value of ω_2 can be calculated from the parity eigenvalues of the occupied bands at TRIM, $k_i \in (\Gamma, M_1, M_2, M_3)$, using the expression:

$$(-1)^{\omega_2} = \prod_{k_i \in \text{TRIM}} (-1)^{\lfloor N_{\text{occ}}^-(k_i)/2 \rfloor},$$

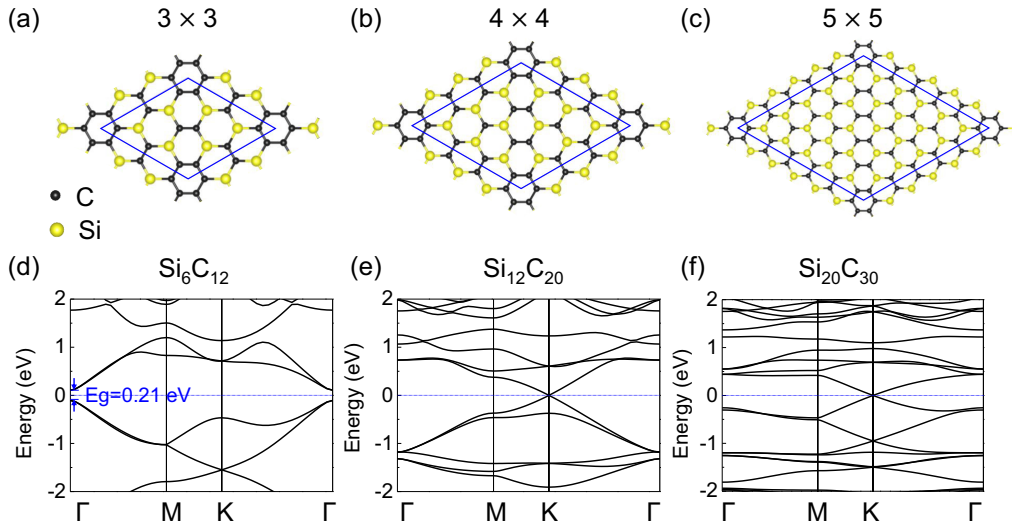

FIG. 2. Atomic structures and band structures of two-dimensional (2D) Si_xC_y. Atomic structures of (a) second-order ($\omega_2 = 1$) and (b) and (c) first-order topological insulators ($\mathbb{Z}_2 = 1$). The black and yellow spheres represent C and Si atoms, respectively. The blue dotted rhombus represent primitive unit cells of the 2D Si_xC_y. The electronic band structures of (d) Si_6C_{12}, (e) $Si_{12}C_{20}$, and (f) $Si_{20}C_{30}$.

where $N^-_{\rm occ}(k_i)$ is the number of occupied bands with an odd parity at k_i, and $\lfloor N^-_{\rm occ}(k_i)/2 \rfloor$ is the floor function, returning the greatest integer less than or equal to $N^-_{\rm occ}(k_i)/2$. The calculated parities at TRIM are listed in Table S1 in the SM [34]. We find that the occupied states at the Γ (M) point have 3 (5) odd bands out of 9, leading to a nonzero $\omega_2 = 1$, which indicates the system with period of (3 × 3) to be a 2D SOTI.

To find out the key roles of the emergence of the SOTI, we analyze the energy dispersion for different ratios of t_2 and t_3 hopping parameters. The system becomes a trivial insulator when $|t_2/t_3| > 1$, as shown in Fig. S1(a) in the SM [34]. As $|t_2/t_3|$ decreases, a topological phase transition occurs at $|t_2/t_3| = 1$. At that critical point, the system becomes a semimetal, as shown in Fig. S1(b) in the SM [34]. A band inversion occurs at the Γ point for smaller $|t_2/t_3|$, leading to a SOTI phase. Moreover, the signs of t_2 and t_3 have no effect on the energy dispersion and band topology of the systems with periods of (3 × 3), which is different from the previous studies [28,29].

III. DISCUSSION

Recent successful synthesis of monolayer honeycomb SiC and Si_9C_{15} indicates the tunable ratio of Si and C atoms [35,36]. The coexistence of Si-C and C-C bonds is promising for the realization of Kekulé distortion in Si_xC_y systems. Using the approach, we propose a family of 2D Si_xC_y to be SOTIs and FOTIs. The structure of optimized freestanding 2D Si_xC_y is completely flat with a single-atom thickness, as shown in Figs. 2(a)–2(c). The space group of Si_xC_y is *P6/mmm*. Consisting of sp^2-hybridized carbon and silicon atoms, 2D Si_xC_y exhibits a high π conjugation, which helps to stabilize the planar structures. The stoichiometric formula of 2D Si_xC_y systems with a period of ($N \times N$), where $N = 3m + l$ ($m = 1, 2, \ldots$; $l = 0, 1, 2$) can be summarized as $x = (3m + l)(3m + l - 1)$, $y = (3m + l)(3m + l + 1)$. Thus, the 2D systems with periods of (3 × 3), (4 × 4), and (5 × 5) have stoichiometric formulas of Si_6C_{12}, $Si_{12}C_{20}$, and $Si_{20}C_{30}$ in each unit cell [blue rhombus in Figs. 2(a)–2(c)], respectively. The averaged lengths of C-C and C-Si bonds in each unit cell are ∼1.44 and 1.81 Å, respectively. The fully relaxed lattice constants of 2D Si_6C_{12}, $Si_{12}C_{20}$, and $Si_{20}C_{30}$ are 8.76, 11.87, and 14.97 Å, respectively. The absence of imaginary frequencies in the phonon dispersion calculations of 2D Si_6C_{12}, $Si_{12}C_{20}$, and $Si_{20}C_{30}$ (see the SM [34], see also Refs. [37–39] therein) indicate they are thermodynamically stable structures.

A global direct band gap of 0.21 eV is formed between the conduction band minimum (CBM) and valence band maximum (VBM) at the Γ point in the 2D Si_6C_{12} structure, as shown in Fig. 2(d). Notably, both the CBM and VBM of the2D Si_6C_{12} structure are doublet degenerate. From the projected density of states (PDOS) shown in Fig. S5(b) in the SM [34], the bands near the Fermi level mainly come from the p_z orbitals of the carbon and silicon atoms in 2D Si_6C_{12}. The VBM is mainly contributed by the central SiC six-rings, while the CBM is contributed by the C six-rings and nearby Si atoms. However, the 2D $Si_{12}C_{20}$ and $Si_{20}C_{30}$ structures both display twofold degenerate Dirac points at the K point without considering spin-orbit coupling (SOC), as shown in Figs. 2(d)–2(f). The calculated $\mathbb{Z}_2$ invariants ($\mathbb{Z}_2 = 1$) indicate $Si_{12}C_{20}$ and $Si_{20}C_{30}$ are FOTIs.

It is interesting to note that the 2D irreducible representations of the CBM and VBM in Si_6C_{12} are E_{2u} and E_{1g}, respectively. The two irreducible representations have opposite parities under inversion symmetry, which is consistent with the band-inversion-induced nontrivial topological states based on the TB model. Moreover, the calculated nonzero bulk topological index ($\omega_2 = 1$) further confirms 2D Si_6C_{12} to be a SOTI. In addition to the bulk topological index, the 2D SOTI is also characterized by a gapped edge state. Here, only the armchair edge is considered, as illustrated in Fig. 3(a), since the zigzag edge will induce edge magnetism in 2D Si_6C_{12}, which is beyond our consideration. The edge state is calculated by using the WANNIER90 package, in which a

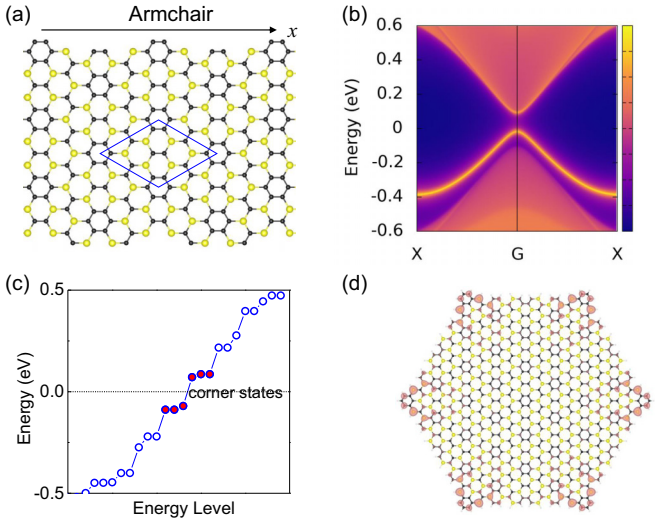

FIG. 3. Topological properties of second-order topological insulator Si_6C_{12}. (a) Semi-infinite structures of armchair-terminated edge. (b) The projected edge density of states. (c) Energy spectrum of the hexagonal-shaped Si_6C_{12} cluster. (d) The total real-space wave function distributions of six in-gap topological corner states. The isosurface is set to be 0.001 *e*/Bohr [3].

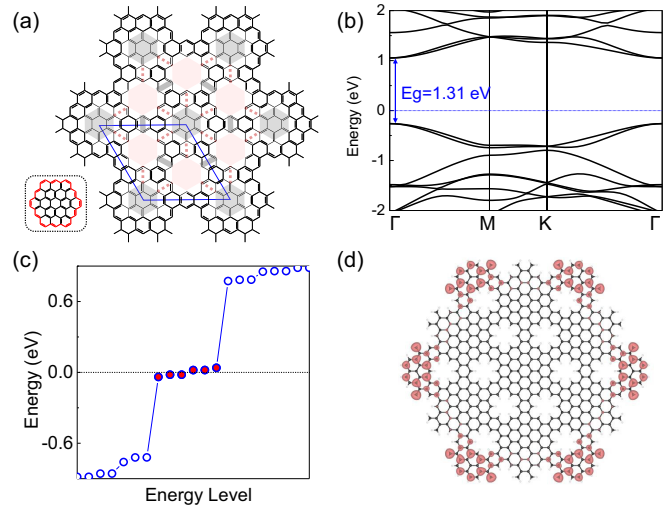

FIG. 4. Topological properties of second-order topological insulator in circumcoronene-based covalent organic framework (COF). (a) Atomic structures and (b) band structure of COF. (c) Energy spectrum of the hexagonal-shaped COF. (d) The total real-space wave function distributions of six in-gap topological corner states. The isosurface is set to be 0.001 *e*/Bohr [3].

TB Hamiltonian in the basis of the maximally localized Wannier functions (MLWFs) is fitted to the first-principles band structure. The Wannier band structure of Si_6C_{12} matches well with the density functional theory (DFT) result (see the SM [34], see also Refs. [40–43] therein). In Fig. 3(b), we plot the edge spectrum for the armchair edge. The calculated results show there is a ∼0.1 eV band gap between the topological edge states, making it possible to detect the in-gap topological corner states experimentally. In addition, the DFT calculated band structure of the Si_6C_{12} nanoribbon also shows a band gap of 0.12 eV (see the SM [34]). The dangling bonds on the edges are saturated with hydrogen atoms. The spatial electron distribution of the VBM and CBM is mainly localized at the armchair edges. Both Wannier and DFT calculations confirm the existence of a gapped edge state.

To further confirm the topological properties of 2D Si_6C_{12}, we calculated the energy spectrum of a finite-sized hexagonal-shaped flake with 780 atoms. To prevent the effect of dangling-bond-related edge states in the gap, we passivated all dangling bonds with hydrogen atoms. The calculated energy spectrum for the flake is plotted in Fig. 3(c). There are six electronic states near the Fermi level, marked by red circles. By plotting the spatial distribution of electron density for these states [Fig. 3(d)], we find that the states are mainly localized on the six corners, which indicates the corner states. Combined with the nontrivial topological invariants and gapped topological edge states, we can firmly identify 2D Si_6C_{12} as a SOTI.

The DFT-calculated band structures and nontrivial topological properties of Si_xC_y systems, where $m = 1$, are consistent with those predicted by our TB models. The rules based on our TB models can also be applied to Si_xC_y systems of $m = 2$, 3, …. In Figs. S8 and S9 in the SM [34], we provide the DFT calculations of 2D Si_xC_y of $m = 2$. Here, 2D $Si_{30}C_{42}$ opened a gap of 0.06 eV at the Γ point. The calculated nonzero bulk topological index ($\omega_2 = 1$) and corner states (see the SM [34]) in a finite-sized hexagonal-shaped flake indicate that it is a SOTI. Also, 2D $Si_{42}C_{56}$ and $Si_{56}C_{72}$ both have Dirac points, and the calculated $\mathbb{Z}_2$ invariants equal 1, confirming the systems remain FOTIs. The two-dimensional Si_2C_6 compound reported by Ding and Wang [44] is a FOTI, which also follows our rule.

We also applied this mechanism to the COF. The chemical structure of the circumcoronene-based COF is shown in Fig. 4(a). The holes in the COF can be viewed as Kekulé-T distortion and honeycomb patterns linked by lines in orange and gray in Fig. 4(a). The DFT-calculated band structure of the circumcoronene-based COF has a global band gap of 1.31 eV at the Γ point, as shown in Fig. 4(b). The calculated nonzero bulk topological index ($\omega_2 = 1$) indicates it to be a 2D SOTI. To further identify corner topology, we calculated the energy spectrum of a finite-sized hexagonal-shaped flake with hydrogen atoms passivating all dangling bonds. The calculated discrete spectrum for the flake is plotted in Fig. 4(c). There are six electronic states near the Fermi level. The electron density distributions of these six electronic states in real space are plotted in Fig. 4(d). Clearly, these states are well localized at the six corners, so they correspond to topological corner states. Combined with the nontrivial topological invariants, we can thus firmly confirm the circumcoronene-based COF is a SOTI.

IV. CONCLUSIONS

In summary, we proposed a general mechanism to realize intrinsic SOTIs in 2D real materials and predicted the existence of second-order topological states in 2D Si_xC_y and the circumcoronene-based COF by using first-principles calculations. These discoveries will draw more fundamental research interest to explore higher-order TIs in 2D electronic materials in the future.

ACKNOWLEDGMENTS

This paper was supported by the National Natural Science Foundation of China (Grants No. 62488201, No. 52201231, and No. 22372047), the National Key Research and Development Program of China (Grants No. 2022YFA1204100 and No. 2019YFA0308500), CAS Project for Young Scientists in Basic Research (Grant No. YSBR-003), and the Fundamental Research Funds for the Central Universities (Grant No. FRF-TP-24–055A).

The authors declare no competing financial interest.

[1] W. A. Benalcazar, B. A. Bernevig, and T. L. Hughes, Electric multipole moments, topological multipole moment pumping, and chiral hinge states in crystalline insulators, Phys. Rev. B **96**, 245115 (2017).

[2] J. Langbehn, Y. Peng, L. Trifunovic, F. von Oppen, and P. W. Brouwer, Reflection-symmetric second-order topological insulators and superconductors, Phys. Rev. Lett. **119**, 246401 (2017).

[3] Z. D. Song, Z. Fang, and C. Fang, (d-2)-Dimensional edge states of rotation symmetry protected topological states, Phys. Rev. Lett. **119**, 246402 (2017).

[4] F. Zhang, C. L. Kane, and E. J. Mele, Surface state magnetization and chiral edge states on topological insulators, Phys. Rev. Lett. **110**, 046404 (2013).

[5] W. A. Benalcazar, B. A. Bernevig, and T. L. Hughes, Quantized electric multipole insulators, Science **357**, 61 (2017).

[6] F. Schindler, A. M. Cook, M. G. Vergniory, Z. J. Wang, S. S. P. Parkin, B. A. Bernevig, and T. Neupert, Higher-order topological insulators, Sci. Adv. **4**, eaat0346 (2018).

[7] B. Y. Xie, H. X. Wang, X. J. Zhang, P. Zhan, J. H. Jiang, M. H. Lu, and Y. F. Chen, Higher-order band topology, Nat. Rev. Phys. **3**, 520 (2021).

[8] F. Schindler, Z. J. Wang, M. G. Vergniory, A. M. Cook, A. Murani, S. Sengupta, A. Y. Kasumov, R. Deblock, S. Jeon, I. Drozdov *et al.*, Higher-order topology in bismuth, Nat. Phys. **14**, 918 (2018).

[9] C. Chen, Z. Song, J.-Z. Zhao, Z. Y. Chen, Z.-M. Yu, X.-L. Sheng, and S. A. Yang, Universal approach to magnetic second-order topological insulator, Phys. Rev. Lett. **125**, 056402 (2020).

[10] Y. F. Ren, Z. H. Qiao, and Q. Niu, Engineering corner states from two-dimensional topological insulators, Phys. Rev. Lett. **124**, 166804 (2020).

[11] C. H. Hsu, X. T. Zhou, T. R. Chang, Q. Ma, N. Gedik, A. Bansil, S. Y. Xu, H. Lin, and L. Fu, Topology on a new facet of bismuth, Proc. Natl. Acad. Sci. USA **116**, 13255 (2019).

[12] M. Ezawa, Higher-order topological insulators and semimetals on the breathing kagome and pyrochlore lattices, Phys. Rev. Lett. **120**, 026801 (2018).

[13] S. F. Qian, C. C. Liu, and Y. G. Yao, Second-order topological insulator state in hexagonal lattices and its abundant material candidates, Phys. Rev. B **104**, 245427 (2021).

[14] H. M. Mu, B. Liu, T. Y. Hu, and Z. F. Wang, Kekulé lattice in graphdiyne: Coexistence of phononic and electronic second-order topological insulator, Nano Lett. **22**, 1122 (2022).

[15] L. Chen, C.-C. Liu, B. Feng, X. He, P. Cheng, Z. Ding, S. Meng, Y. Yao, and K. Wu, Evidence for Dirac fermions in a honeycomb lattice based on silicon, Phys. Rev. Lett. **109**, 056804 (2012).

[16] A. H. Castro Neto, F. Guinea, N. M. R. Peres, K. S. Novoselov, and A. K. Geim, The electronic properties of graphene, Rev. Mod. Phys. **81**, 109 (2009).

[17] C. H. Park and S. G. Louie, Making massless Dirac fermions from a patterned two-dimensional electron gas, Nano Lett. **9**, 1793 (2009).

[18] S. H. Lee, H. J. Chung, J. Heo, H. Yang, J. Shin, U. I. Chung, and S. Seo, Band gap opening by two-dimensional manifestation of Peierls instability in graphene, ACS Nano **5**, 2964 (2011).

[19] Z. N. Lin, W. Qin, J. Zeng, W. Chen, P. Cui, J. H. Cho, Z. H. Qiao, and Z. Y. Zhang, Competing gap opening mechanisms of monolayer graphene and graphene nanoribbons on strong topological insulators, Nano Lett. **17**, 4013 (2017).

[20] I. F. Herbut, V. Juricic, and B. Roy, Theory of interacting electrons on the honeycomb lattice, Phys. Rev. B **79**, 085116 (2009).

[21] Y. Ren, X. Deng, Z. Qiao, C. Li, J. Jung, C. Zeng, Z. Zhang, and Q. Niu, Single-valley engineering in graphene superlattices, Phys. Rev. B **91**, 245415 (2015).

[22] C. H. Bao, H. Y. Zhang, T. Zhang, X. Wu, L. P. Luo, S. H. Zhou, Q. Li, Y. H. Hou, W. Yao, L. W. Liu *et al.*, Experimental evidence of chiral symmetry breaking in Kekulé-ordered graphene, Phys. Rev. Lett. **126**, 206804 (2021).

[23] Y. Liu, C.-S. Lian, Y. Li, Y. Xu, and W. H. Duan, Pseudospins and topological effects of phonons in a Kekulé lattice, Phys. Rev. Lett. **119**, 255901 (2017).

[24] C. Gutierrez, C. J. Kim, L. Brown, T. Schiros, D. Nordlund, E. B. Lochocki, K. M. Shen, J. Park, and A. N. Pasupathy, Imaging chiral symmetry breaking from Kekulé bond order in graphene, Nat. Phys. **12**, 950 (2016).

[25] F. Liu, M. Yamamoto, and K. Wakabayashi, Topological edge states of honeycomb lattices with zero Berry curvature, J. Phys. Soc. Jpn. **86**, 123707 (2017).

[26] Y. Xue, H. Huan, B. Zhao, Y. Luo, Z. Zhang, and Z. Yang, Higher-order topological insulators in two-dimensional Dirac materials, Phys. Rev. Res. **3**, L042044 (2021).

[27] T. Y. Hu, T. F. Zhang, H. M. Mu, and Z. F. Wang, Intrinsic second-order topological insulator in two-dimensional covalent organic frameworks, J. Phys. Chem. Lett. **13**, 10905 (2022).

[28] X. J. Ni, H. Q. Huang, and J. L. Bredas, Organic higher-order topological insulators: Heterotriangulene-based covalent organic frameworks, J. Am. Chem. Soc. **144**, 22778 (2022).

[29] B. Liu, G. Zhao, Z. Liu, and Z. F. Wang, Two-dimensional quadrupole topological insulator in γ-graphyne, Nano Lett. **19**, 6492 (2019).

[30] E. W. Lee, R. Kim, J. Ahn, and B. J. Yang, Two-dimensional higher-order topology in monolayer graphdiyne, npj Quantum Mater. **5**, 1 (2020).

[31] C. Chen, W. K. Wu, Z.-M. Yu, Z. Chen, Y. X. Zhao, X.-L. Sheng, and S. A. Yang, Graphyne as a second-order and real Chern topological insulator in two dimensions, Phys. Rev. B **104**, 085205 (2021).

[32] X.-L. Sheng, C. Chen, H. Liu, Z. Chen, Z.-M. Yu, Y. X. Zhao, and S. A. Yang, Two-dimensional second-order topological insulator in graphdiyne, Phys. Rev. Lett. **123**, 256402 (2019).

[33] O. V. Gamayun, V. P. Ostroukh, N. V. Gnezdilov, I. Adagideli, and C. W. J. Beenakker, Valley-momentum locking in a graphene superlattice with Y-shaped Kekulé bond texture, New J. Phys. **20**, 023016 (2018).

[34] See Supplemental Material at http://link.aps.org/supplemental/10.1103/PhysRevB.110.125103 for discussion about the TB calculated parities and band structures of honeycomb lattices. The effect of on-site energy in the TB model is also discussed. In addition, DFT-calculated parities, phonon dispersions, and band structures of structures are also provided.

[35] C. M. Polley, H. Fedderwitz, T. Balasubramanian, A. A. Zakharov, R. Yakimova, O. Bäcke, J. Ekman, S. P. Dash, S. Kubatkin, and S. Lara-Avila, Bottom-up growth of monolayer honeycomb SiC, Phys. Rev. Lett. **130**, 076203 (2023).

[36] Z. Y. Gao, W. P. Xu, Y. X. Gao, R. Guzman, H. Guo, X. Y. Wang, Q. Zheng, Z. L. Zhu, Y. Y. Zhang, X. Lin *et al.*, Experimental realization of atomic monolayer Si_9C_{15}, Adv. Mater. **34**, 2204779 (2022).

[37] G. Kresse and J. Furthmuller, Efficient iterative schemes for *ab initio* total-energy calculations using a plane-wave basis set, Phys. Rev. B **54**, 11169 (1996).

[38] J. P. Perdew, K. Burke, and M. Ernzerhof, Generalized gradient approximation made simple, Phys. Rev. Lett. **77**, 3865 (1996).

[39] A. Togo and I. Tanaka, First principles phonon calculations in materials science, Scr. Mater. **108**, 1 (2015).

[40] A. A. Mostofi, J. R. Yates, Y. S. Lee, I. Souza, D. Vanderbilt, and N. Marzari, WANNIER90: A tool for obtaining maximally-localised Wannier functions, Comput. Phys. Commun. **178**, 685 (2008).

[41] A. A. Mostofi, J. R. Yates, G. Pizzi, Y. S. Lee, I. Souza, D. Vanderbilt, and N. Marzari, An updated version of WANNIER90: A tool for obtaining maximally-localised Wannier functions, Comput. Phys. Commun. **185**, 2309 (2014).

[42] Q. S. Wu, S. N. Zhang, H. F. Song, M. Troyer, and A. A. Soluyanov, WANNIERTOOLS: An open-source software package for novel topological materials, Comput. Phys. Commun. **224**, 405 (2018).

[43] J. C. Gao, Q. S. Wu, C. Persson, and Z. J. Wang, IRVSP: To obtain irreducible representations of electronic states in the VASP, Comput. Phys. Commun. **261**, 107760 (2021).

[44] Y. Ding and Y. L. Wang, Geometric and electronic structures of two-dimensional SiC compound, J. Phys. Chem. C **118**, 4509 (2014).